Identification of LRRC8 Heteromers as an Essential Component of the Volume-Regulated Anion Channel VRAC

Felizia K. Voss *et al.*

Science **344**, 634 (2014);
DOI: 10.1126/science.1252826

References and Notes

1. Q. Shen *et al.*, *Science* **304**, 1338–1340 (2004).
2. M. Tavazoie *et al.*, *Cell Stem Cell* **3**, 279–288 (2008).
3. T. Shingo *et al.*, *Science* **299**, 117–120 (2003).
4. P. Wu *et al.*, *Neurobiol. Aging* **29**, 1502–1511 (2008).
5. H. van Praag, G. Kempermann, F. H. Gage, *Nat. Neurosci.* **2**, 266–270 (1999).
6. J. S. Snyder, A. Soumier, M. Brewer, J. Pickel, H. A. Cameron, *Nature* **476**, 458 (2011).
7. E. Farkas, P. G. Luiten, *Prog. Neurobiol.* **64**, 575–611 (2001).
8. H. G. Kuhn, H. Dickinson-Anson, F. H. Gage, *J. Neurosci.* **16**, 2027–2033 (1996).
9. T. Seki, Y. Arai, *Neuroreport* **6**, 2479–2482 (1995).
10. S. A. Villeda *et al.*, *Nature* **477**, 90–94 (2011).
11. J. M. Ruckh *et al.*, *Cell Stem Cell* **10**, 96–103 (2012).
12. V. E. Miron *et al.*, *Nat. Neurosci.* **16**, 1211–1218 (2013).
13. F. S. Loffredo *et al.*, *Cell* **153**, 828–839 (2013).
14. D. E. Wright, A. J. Wagers, A. P. Gulati, F. L. Johnson, I. L. Weissman, *Science* **294**, 1933–1936 (2001).
15. T. Seki, *J. Neurosci. Res.* **70**, 327–334 (2002).
16. A. Garcia, B. Steiner, G. Kronenberg, A. Bick-Sander, G. Kempermann, *Aging Cell* **3**, 363–371 (2004).
17. J. Luo, S. B. Daniels, J. B. Lennington, R. Q. Notti, J. C. Conover, *Aging Cell* **5**, 139–152 (2006).
18. V. Tropepe, C. G. Craig, C. M. Morshead, D. van der Kooy, *J. Neurosci.* **17**, 7850–7859 (1997).
19. B. A. Reynolds, S. Weiss, *Science* **255**, 1707–1710 (1992).
20. L. Katsimpardi *et al.*, *Stem Cells* **26**, 1796–1807 (2008).
21. A. Carleton, L. T. Petreanu, R. Lansford, A. Alvarez-Buylla, P. M. Lledo, *Nat. Neurosci.* **6**, 507–518 (2003).
22. R. M. Witt, M. M. Galligan, J. R. Despinoy, R. Segal, *J. Vis. Exp.* **28**, 949 (2009).
23. M. J. Reed, J. M. Edelberg, *Sci. SAGE KE* **2004**, pe7 (2004).
24. A. Rivard *et al.*, *Circulation* **99**, 111–120 (1999).
25. D. R. Riddle, W. E. Sonntag, R. J. Lichtenwalner, *Ageing Res. Rev.* **2**, 149–168 (2003).
26. C. L. Grady *et al.*, *Neuroimage* **8**, 409–425 (1998).
27. R. Balabanov, P. Dore-Duffy, *J. Neurosci. Res.* **53**, 637–644 (1998).
28. P. Carmeliet, *Nat. Rev. Genet.* **4**, 710–720 (2003).
29. A. Alvarez-Buylla, D. A. Lim, *Neuron* **41**, 683–686 (2004).
30. M. Brines, A. Cerami, *Nat. Rev. Neurosci.* **6**, 484–494 (2005).
31. E. R. Matarredona, M. Murillo-Carretero, B. Moreno-López, C. Estrada, *Brain Res. Brain Res. Rev.* **49**, 355–366 (2005).
32. M. Sinha *et al.*, *Science* **344**, 649–652 (2014).

Acknowledgments: We thank C. McGillivray and D. Faria at the HSCRB Histology Core for providing help with sectioning and D. Smith and B. Götze at the HCBI for providing microscope facilities. We also thank W. Stallcup for providing the anti-NG2 antibody, C. Bonal for technical help and J. LaLonde for editorial assistance. This work was supported by a Senior Scholar in Aging Award from The Ellison Medical Foundation to L.L.R.; awards from GlaxoSmithKline and the Harvard Stem Cell Institute to L.L.R.; NIH (R01 AG032977 1R01 AG040019) to R.T.L.; and the Paul F. Glenn Foundation for Medical Research, NIH (1R01 AG033053, 1DP2 OD004345, and 5U01 HL100402), and Harvard Stem Cell Institute to A.J.W. Additional data are in the Supplement. J.C. was funded by NIH R01NS070835 and R01NS072167. L.L.R., A.J.W., R.T.L., and L.K. are inventors on a U.S. patent application filed by Harvard University and Brigham and Women's Hospital entitled "Methods and Compositions for Increasing Neurogenesis and Angiogenesis" (61/833,813).

Supplementary Materials

www.sciencemag.org/content/344/6184/630/suppl/DC1
Materials and Methods
Figs. S1 to S12
References (*33*–*34*)

22 January 2014; accepted 10 April 2014
10.1126/science.1251141

Identification of LRRC8 Heteromers as an Essential Component of the Volume-Regulated Anion Channel VRAC

Felizia K. Voss,[1,2,3] Florian Ullrich,[1,2,3] Jonas Münch,[1,2,3] Katina Lazarow,[1] Darius Lutter,[1,2,3] Nancy Mah,[2] Miguel A. Andrade-Navarro,[2] Jens P. von Kries,[1] Tobias Stauber,[1,2]* Thomas J. Jentsch[1,2,4]*

Regulation of cell volume is critical for many cellular and organismal functions, yet the molecular identity of a key player, the volume-regulated anion channel VRAC, has remained unknown. A genome-wide small interfering RNA screen in mammalian cells identified LRRC8A as a VRAC component. LRRC8A formed heteromers with other LRRC8 multispan membrane proteins. Genomic disruption of *LRRC8A* ablated VRAC currents. Cells with disruption of all five *LRRC8* genes required LRRC8A cotransfection with other LRRC8 isoforms to reconstitute VRAC currents. The isoform combination determined VRAC inactivation kinetics. Taurine flux and regulatory volume decrease also depended on LRRC8 proteins. Our work shows that VRAC defines a class of anion channels, suggests that VRAC is identical to the volume-sensitive organic osmolyte/anion channel VSOAC, and explains the heterogeneity of native VRAC currents.

Cells regulate their volume to counteract swelling or shrinkage caused by osmotic challenges and during processes such as cell growth, division, and migration. As water transport across cellular membranes is driven by osmotic gradients, cell volume regulation requires appropriate changes of intracellular concentrations of ions or organic osmolytes such as taurine (*1*, *2*). Regulatory volume decrease (RVD) follows the extrusion of intracellular Cl^- and K^+ and other osmolytes across the plasma membrane. A key player is the volume-regulated anion channel VRAC that mediates characteristic swelling-activated Cl^- currents [$I_{Cl(swell)}$] and is ubiquitously expressed in vertebrate cells (*3*–*5*). Nearly inactive under resting conditions, VRAC slowly opens upon hypotonic swelling. The mechanism behind VRAC opening remains enigmatic. VRAC currents are outwardly rectifying [hence the alternative name VSOR for volume-stimulated outward rectifier (*4*, *5*)] and show variable inactivation at inside-positive voltages. VRAC conducts iodide (I^-) better than chloride (Cl^-) and might also conduct organic osmolytes such as taurine (*6*) [hence VSOAC, volume-stimulated organic osmolyte/anion channel (*7*)], but this notion is controversial (*8*–*10*). VRAC is believed to be important for cell volume regulation and swelling-induced exocytosis (*11*) and also for cell cycle regulation, proliferation, and migration (*1*, *3*, *4*). It may play a role in apoptosis and various pathological states, including ischemic brain edema and cancer (*4*, *12*). Progress in the characterization of VRAC and its biological roles has been limited by the failure to identify the underlying protein(s) despite decades of efforts (*1*, *5*). ClC-2 Cl^- channels activate upon cell swelling, but their inward rectification and Cl^- over I^- selectivity deviate from VRAC (*13*). *Drosophila* dBest1, a member of a family of Ca^{2+}-activated Cl^- channels, mediates swelling-activated Cl^- currents in insect cells (*14*, *15*), but their characteristics differ from those of VRAC currents, and the mammalian homolog of dBest1 is swelling-insensitive (*16*). We show that VRAC represents a distinct class of anion channels that also conduct organic osmolytes.

To identify VRAC, we used a genome-wide RNA interference screen that could identify nonredundant VRAC components. Swelling-induced I^- influx into human embryonic kidney (HEK) cells expressing the I^--sensitive yellow fluorescent protein YFP(H148Q/I152L) (*17*) was used as readout in a fluorometric imaging plate reader (Fig. 1A). Exposure to saline containing 50 mM I^- yielded a slow fluorescence decay under isotonic conditions, whereas hypotonicity induced a delayed increase in YFP quenching (Fig. 1B) that could be reduced by VRAC inhibitors such as carbenoxolone (*18*) (fig. S1). In a prescreen targeting 21 anion transporters (table S1), only small interfering RNAs (siRNAs) against the Cl^-/HCO_3^- exchanger AE2 gave significant effects (Fig. 1B). They decreased I^- influx under both isotonic and hypotonic conditions.

Our genome-wide screen used three separately transfected siRNAs per gene (fig. S2). Offline data analysis (fig. S3, A and B) yielded the maximal slope of fluorescence quenching that was used to define hits. Further criteria included the presence of predicted transmembrane domains and a wide expression pattern. Eighty-seven genes (table S2) were taken into a secondary screen with independent siRNAs. Of these, only sup-

[1]Leibniz-Institut für Molekulare Pharmakologie (FMP), Berlin. [2]Max-Delbrück-Centrum für Molekulare Medizin (MDC), Berlin. [3]Graduate Program of the Freie Universität Berlin. [4]Neurocure, Charité Universitätsmedizin, Berlin.

*Corresponding author. E-mail: jentsch@fmp-berlin.de (T.J.J.); tstauber@fmp-berlin.de (T.S.)

pression of leucine-rich repeat–containing 8A (LRRC8A) robustly slowed hypotonicity-induced YFP quenching (Fig. 1C). *LRRC8A* knockdown also strongly suppressed $I_{Cl(swell)}$ in patch-clamp experiments (Fig. 1, D to F), suggesting that the multispan membrane protein LRRC8A is an indispensable component of VRAC or is needed for its activation.

Although LRRC8A reached the plasma membrane (Fig. 1G, and fig. S4A for HeLa cells), its transfection into HEK cells rather decreased $I_{Cl(swell)}$ (Fig. 1F). We hypothesized that VRAC contains LRRC8A as part of a heteromer and that LRRC8A overexpression led to a subunit stoichiometry that was incompatible with channel activity. LRRC8A has four closely related homologs (LRRC8B to LRRC8E), which all have four predicted transmembrane domains (*19*, *20*). Expressed sequence tag (EST) databases suggested that all homologs were widely expressed. Immunocytochemistry of transfected HeLa cells (fig. S4A) and of native HEK cells (Fig. 1, G and H) detected LRRC8A at the plasma membrane. Truncation of its C terminus, as in a patient with agammaglobulinemia (*21*), led to cytoplasmic retention (fig. S4B). LRRC8B through LRRC8E remained intracellular when transfected alone, but reached the plasma membrane when cotransfected with LRRC8A (Fig. 1, I and J, and fig. S4, C to H). Unlike LRRC8A transfection, LRRC8A and LRRC8C coexpression did not suppress $I_{Cl(swell)}$ (Fig. 1F). However, neither this coexpression, nor any other combination tested, significantly increased current amplitudes above wild-type (WT) values.

We used zinc-finger nuclease and clustered regularly interspaced short palindromic repeats (CRISPR)–Cas (*22*) technologies to constitutively disrupt *LRRC8* genes. In addition to polyploid HEK cells, we used stably diploid human HCT116 cells for increased disruption efficiency. Gene disruption was confirmed by sequencing and Western blots (Fig. 2A and table S3). To exclude off-target effects, we generated two HEK and three HCT116 lines in which *LRRC8A* was disrupted at different positions (tables S3 and S4). $I_{Cl(swell)}$ was abolished in all five lines and could be rescued by LRRC8A transfection (Fig. 2, B and C, and fig. S5), demonstrating that LRRC8A is essential for $I_{Cl(swell)}$. We also produced HCT116 cells in which other *LRRC8* genes were disrupted singly or in combinations, including a line with disruption of all five *LRRC8* genes (henceforth called *LRRC8*$^{-/-}$ cells). Except for *LRRC8A*, disruption of single *LRRC8* genes did not abolish VRAC currents (Fig. 2, B and C). However, $I_{Cl(swell)}$ amplitudes were robustly reduced in *LRRC8E*$^{-/-}$ and in *LRRC8(C/E)*$^{-/-}$ double and *LRRC8(C/D/E)*$^{-/-}$ triple knockout (KO) cells. $I_{Cl(swell)}$ was abolished in *LRRC8(B/C/D/E)*$^{-/-}$ cells (Fig. 2, B and C). $I_{Cl(swell)}$ inactivated faster and at less positive potentials in *LRRC8C*$^{-/-}$ and *LRRC8(C/E)*$^{-/-}$ cells compared to WT HCT116, *LRRC8B*$^{-/-}$, *LRRC8D*$^{-/-}$, or *LRRC8E*$^{-/-}$ cells. By contrast, $I_{Cl(swell)}$ inactivated more slowly and at more positive voltages in *LRRC8(D/E)*$^{-/-}$ HTC116 cells (Fig. 2, B and D, and fig. S6D) and in WT HEK cells (Figs. 1E and 2D). $I_{Cl(swell)}$ of these mutant cell lines retained the ion selectivity of WT VRAC with the characteristic $I^- > NO_3^- > Cl^- >> Glc^-$ (gluconate) permeability sequence (fig. S6A).

LRRC8A transfection into quintuple KO *LRRC8*$^{-/-}$ cells failed to rescue $I_{Cl(swell)}$ (Fig. 2, E and F), agreeing with the absence of $I_{Cl(swell)}$ in *LRRC8(B/C/D/E)*$^{-/-}$ cells (Fig. 2, B and C). Cotransfecting *LRRC8*$^{-/-}$ cells with LRRC8A and either LRRC8C or LRRC8E yielded $I_{Cl(swell)}$ with current densities similar to those of native cells (Fig. 2F). Coexpressing LRRC8A with LRRC8D yielded lower currents (Fig. 2, E and F). No current was observed upon coexpression of LRRC8A and LRRC8B, which may relate to the poor expression of LRRC8B (Fig. 3, D and F). These findings are consistent with the low currents observed in *LRRC8(C/E)*$^{-/-}$ cells (Fig. 2C), where LRRC8A can only interact with poorly expressed LRRC8B and/or LRRC8D. Reconstituted $I_{Cl(swell)}$ activated similarly to WT VRAC

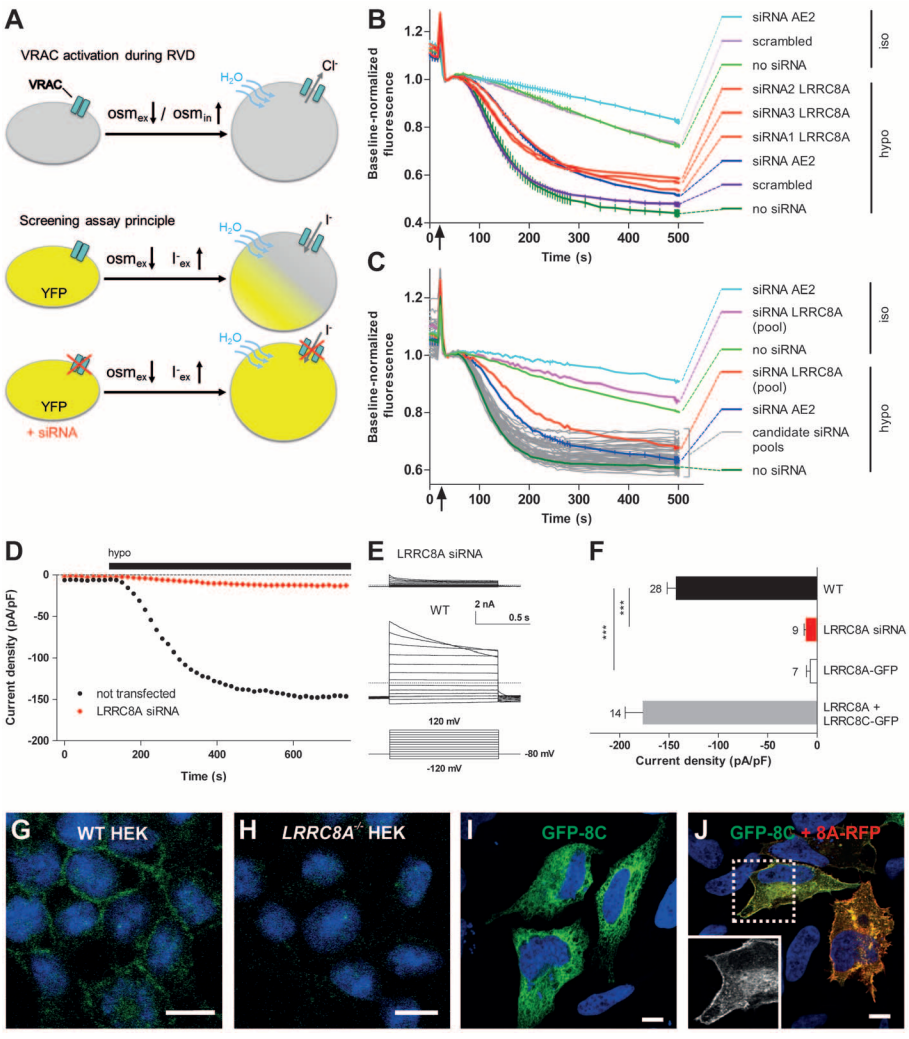

Fig. 1. siRNA screen for volume-regulated anion channel VRAC identifies LRRC8A. (**A**) Principle of screen. Top: In regulatory volume decrease (RVD), VRAC releases Cl^-. Bottom: Quenching of YFP fluorescence by I^- entering through VRAC used as readout. (**B**) Example traces, normalized to fluorescence at ~30 to 50 s. Traces averaged from wells treated with control siRNAs (scrambled, AE2, both $n = 3$) and no siRNA ($n = 2$) (error bars, SEM), and individual traces from wells singly transfected with the three siRNAs against LRRC8A. Except for LRRC8A siRNA2 and 3, all traces are from the same plate. Arrow indicates addition of I^--containing hypotonic (hypo; 229 mOsm) or isotonic (iso; 329 mOsm) saline. (**C**) Secondary screen using siRNA pools against candidate genes. Averaged control traces as in (B). (**D**) Typical time course of VRAC activation in WT or LRRC8A siRNA-treated HEK cells. Current densities at −80 mV are shown. Bar, application of hypotonic (240 mOsm) saline (hypo). (**E**) Current traces of fully activated $I_{Cl(swell)}$ measured with the protocol shown below. Dotted lines indicate zero current. (**F**) $I_{Cl(swell)}$ amplitudes (at −80 mV) of WT HEK cells, cells treated with LRRC8A siRNA, or transfected with indicated LRRC8 cDNAs. Error bars, SEM; number of experiments is indicated; ***$P < 0.001$. (**G**) Plasma membrane localization of endogenous LRRC8A in HEK cells. (**H**) No LRRC8 labeling in *LRRC8A*$^{-/-}$ HEK cells. (**I**) LRRC8C is intracellular when transfected into HeLa cells, but (**J**) reaches the plasma membrane when cotransfected with LRRC8A. (Inset) Magnification of boxed area showing only GFP fluorescence. Scale bars, 10 μm.

upon swelling (Fig. 2E) and displayed its typical anion permeability sequence (fig. S6, B and C).

$I_{Cl(swell)}$ inactivated more slowly and at more positive voltages when LRRC8A was coexpressed with LRRC8C in *LRRC8*$^{-/-}$ cells compared to cells coexpressing LRRC8A with LRRC8E or LRRC8D (Fig. 2, E and G, and fig. S6E). This observation was in agreement with the faster $I_{Cl(swell)}$ inactivation in *LRRC8C*$^{-/-}$ cells (Fig. 2, B and D, and fig. S6D) in which the "decelerating" LRRC8C subunit may be replaced by LRRC8E or other "accelerating" subunits.

Native $I_{Cl(swell)}$ currents display different inactivation kinetics (*3*). Whereas $I_{Cl(swell)}$ shows prominent inactivation at positive potentials in HEK cells (*23*, *24*) (Fig. 1E, Fig. 2D, and fig. S6D) and even more inactivation in HCT116 cells (Fig. 2, B and D, and fig. S6D), it inactivates much less in blood cells such as promyelocytic HL-60 cells and in vascular smooth muscle and neurons (*24*–*26*). EST databases suggest that these cells express the "decelerating" subunit LRRC8C, but lack LRRC8E that potently induces inactivation (Fig. 2, E and G, and fig. S6E). Quantitative reverse transcription–polymerase chain reaction confirmed that HEK and HCT116 cells expressed LRRC8A through LRRC8E, whereas LRRC8E was almost absent from HL-60 cells (fig. S7). Moreover, HCT116 cells, whose $I_{Cl(swell)}$ inactivates to a greater extent than that of HEK cells (Fig. 1E, Fig. 2, B and D, and fig. S6D), express less "decelerating" LRRC8C than HEK (fig. S7).

LRRC8 proteins have four predicted transmembrane domains (TMDs) followed by hydrophilic C termini with up to 17 leucine-rich repeats (*27*) (Fig. 3A). Their C termini were originally thought to be extracellular (*19*, *21*), but proteome databases revealed (*20*) that the TMD2-TMD3 linker can be phosphorylated and suggested that LRRC8 N and C termini are cytoplasmic (Fig. 3A). LRRC8 proteins display weak homology (*20*) to pannexins, pore-forming proteins (*28*) with

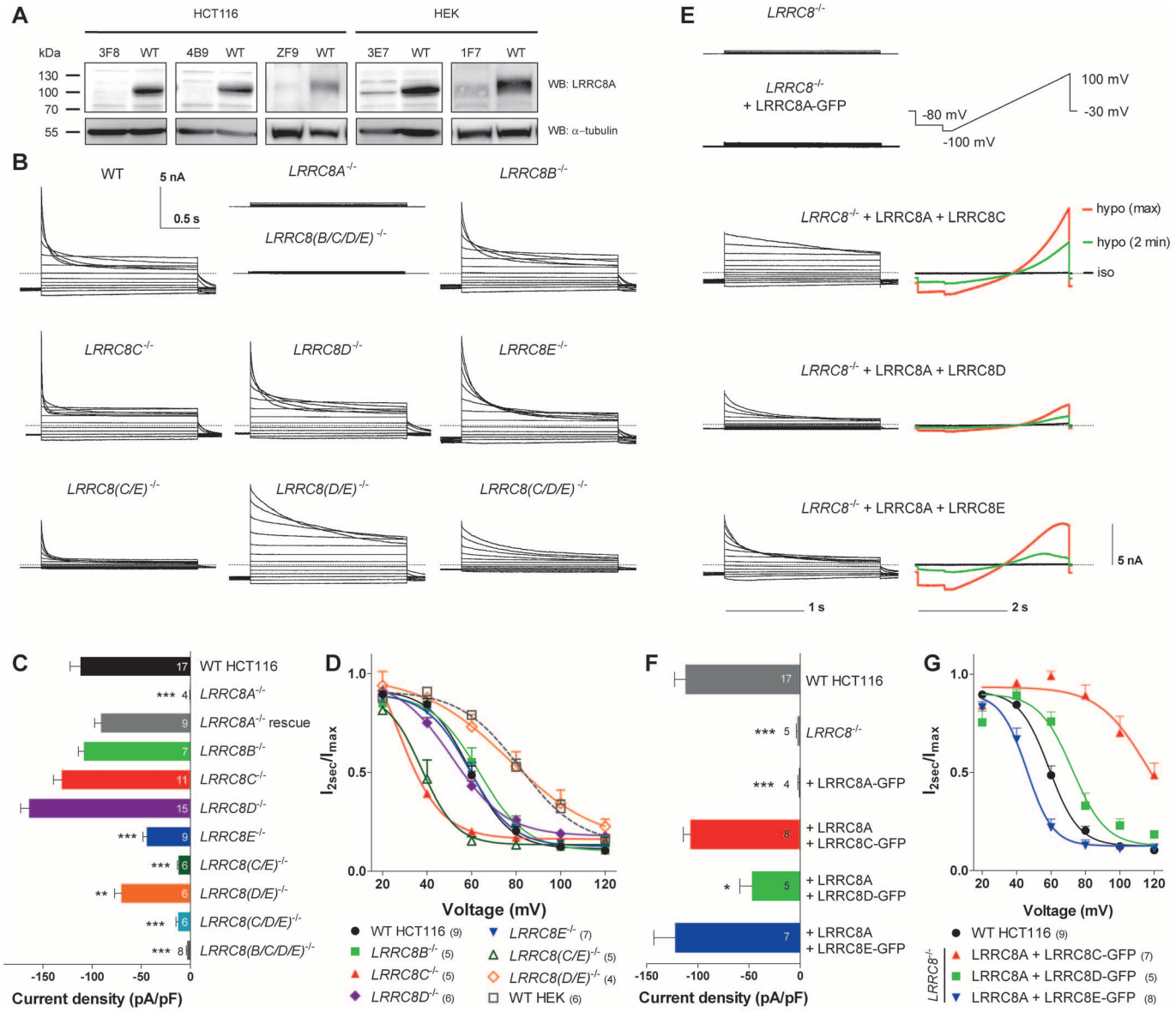

Fig. 2. Characterization of *LRRC8* KO cells and of reconstituted $I_{Cl(swell)}$. (**A**) Western blots confirm *LRRC8A* disruption in mutant cell lines (table S3). α-Tubulin, loading control. (**B**) Example $I_{Cl(swell)}$ traces (as in Fig. 1E, but 2-s pulses) of WT and mutant HCT116 cells. (**C**) Current densities (at –80 mV) of maximally activated $I_{Cl(swell)}$ of WT and mutant HCT116 cells. (**D**) $I_{Cl(swell)}$ inactivation assessed by ratio of current at end and beginning of pulse. (**E**) When transfected into HCT116 *LRRC8*$^{-/-}$ cells (with all *LRRC8* genes disrupted), LRRC8A rescues $I_{Cl(swell)}$ only with LRRC8C, D, or E [left panels; example traces measured as in (B)]. Right panels, example ramp current traces from reconstituted $I_{Cl(swell)}$ at isotonicity (black), 2 min after switching to hypotonicity (green) and with maximal activation (red). Ramp protocol shown at top. (**F**) $I_{Cl(swell)}$ current densities at –80 mV for indicated combinations. (**G**) Voltage-dependent inactivation of $I_{Cl(swell)}$. Error bars, SEM. Number of cells is shown in parentheses. *P < 0.05, **P < 0.01, and ***P < 0.001 versus WT.

connexin-like topology. Connexins form hexameric hemichannels and gap junctions (*29*). This similarity suggested (*20*) that LRRC8 proteins form hexameric channels for as yet unknown substrates. Like VRAC currents (*14*, *15*, *30*), LRRC8 proteins are found in vertebrates but not in other phyla such as arthropoda (*20*).

We ascertained the pannexin- and connexin-like transmembrane topology of LRRC8A. Mutating potential N-linked glycosylation sites between TMD1 and TMD2 abolished the size shift upon PNGaseF treatment (Fig. 3B), demonstrating that this loop is extracellular. Immunofluorescence of cells transfected with hemagglutinin (HA)–tagged LRRC8A constructs showed that the TMD3-4 segment is extracellular and the C terminus cytoplasmic (Fig. 3C).

The formation of LRRC8 heteromers was confirmed by coimmunoprecipitation from HEK cells transfected with LRRC8A and epitope-tagged versions of either LRRC8B, C, D, or E. LRRC8A coprecipitated each of the other isoforms, but not the Cl^- channel ClC-1 used as a control (Fig. 3, D and E). Conversely, precipitation of epitope-tagged versions of LRRC8B through LRRC8E coprecipitated LRRC8A (Fig. 3F). Coprecipitation of LRRC8 isoforms was also observed for native HEK cells (fig. S8).

Hypotonicity induced a robust taurine efflux from HEK and HCT116 cell lines, but not from their *LRRC8A*$^{-/-}$ derivates (Fig. 4A and fig. S9A), where taurine efflux could be rescued by LRRC8A and LRRC8C cotransfection (fig. S9B for HEK cells). Taurine efflux was also abolished in *LRRC8(B/C/D/E)*$^{-/-}$ HCT116 cells (Fig. 4A). Because both $I_{Cl(swell)}$ and swelling-induced taurine efflux similarly depended on LRRC8 heteromers, VRAC is most likely identical to VSOAC, the volume-sensitive organic osmolyte/anion channel (*7*). Accordingly, *LRRC8A*$^{-/-}$ HEK cells showed severely impaired volume regulation. After initial swelling, WT, but not *LRRC8A*$^{-/-}$, cells slowly reduced their volume in the continuous presence of extracellular hypotonicity (Fig. 4B). Hence, LRRC8-containing VSOAC plays a major role in RVD.

The absence of $I_{Cl(swell)}$ upon genomic disruption of *LRRC8A* and its rescue by transient reexpression identified LRRC8A as an indispensable component of VRAC, or alternatively, as being crucial for its activation. The wide expression pattern of *LRRC8* genes and the plasma membrane residency of LRRC8A-containing heteromers fulfill the prerequisites for LRRC8 proteins forming the channel. The dependence of current properties on LRRC8 isoform combinations indicated that LRRC8 heteromers are integral components

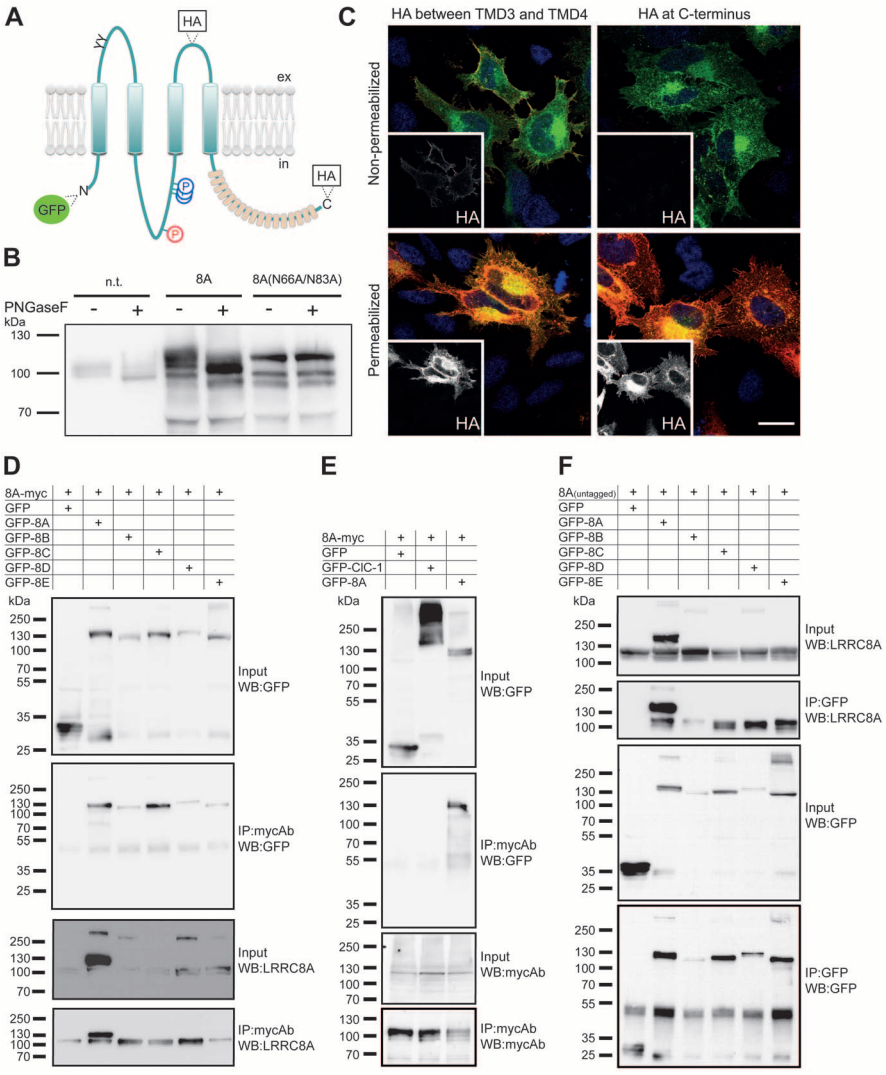

Fig. 3. Transmembrane topology and heteromerization of LRRC8A. (**A**) LRRC8 model [modified from (*20*)]. Four transmembrane domains precede a C terminus with up to 17 leucine-rich repeats (*27*) (orange). Phosphoserines in LRRC8A (red P) and LRRC8D (blue P), according to Uniprot (*32*), predicted N-linked glycosylation sites (Y), and added epitopes are indicated. (**B**) PNGaseF treatment of endogenous LRRC8A, transfected LRRC8A, but not of LRRC8A(N66A,N83A) with disrupted glycosylation sites, decreased LRRC8A size in Western blots. The changed banding pattern of LRRC8A(N66A,N83A) suggests altered posttranslational modifications. n.t., nontransfected. (**C**) Immunofluorescence of nonpermeabilized and permeabilized HeLa cells transfected with HA-tagged GFP-LRRC8A. Overlays of GFP (green) and HA (red) labeling. Insets show exclusively HA staining. Scale bar, 20 μm. (**D**) LRRC8A coprecipitated epitope-tagged LRRC8B through LRRC8E in double-transfected HEK cells. LRRC8B and LRRC8D were poorly expressed. (**E**) LRRC8A did not coprecipitate the ClC-1 Cl^- channel. (**F**) Epitope-tagged LRRC8B through LRRC8E coprecipitated LRRC8A.

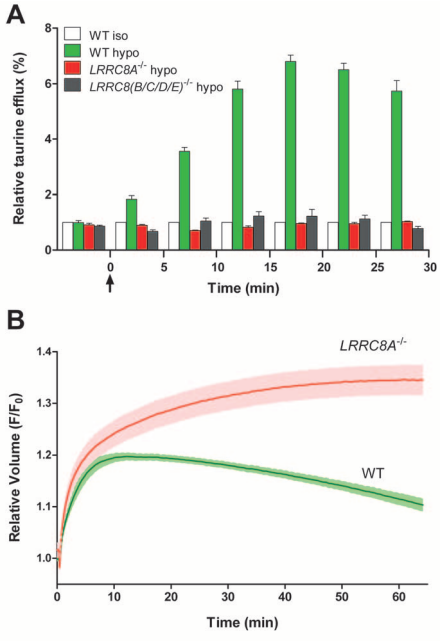

Fig. 4. LRRC8 proteins are crucial for swelling-induced taurine efflux and RVD. (**A**) ^{3}[H]-Taurine efflux from HCT116 cells of indicated genotypes. Cells were either in isotonic solution throughout (WT, white bars) or exposed to hypotonic solution starting at $t = 0$ (arrows). Bars, means of six measurements; error bars, SEM. (**B**) WT and *LRRC8A*$^{-/-}$ HEK cells were shifted to hypotonic saline (96 mOsm) at t = 30s, and cell volume was monitored by calcein fluorescence. Mean of six measurements; error range, SEM. Similar results were obtained in three experiments.

of VRAC, a notion buttressed by the homology of LRRC8 proteins to pannexins. Because cotransfection of LRRC8 isoforms did not significantly increase $I_{Cl(swell)}$ amplitude over that of the WT, other factors limit VRAC activity; for example, an auxiliary subunit of VRAC or part of the signaling cascade leading to its activation. Indeed, VRAC currents seem to be highly regulated, with amplitudes differing by a factor of only 2 to 3 across cell types (*3*, *30*).

The homology between LRRC8 proteins and pannexins suggested that LRRC8 proteins form hexameric channels (*20*). We confirmed the pannexin-like topology of LRRC8A and propose that VRAC is formed by LRRC8 hexamers of LRRC8A and at least one other family member. In this model, VRAC may contain two to five different LRRC8 isoforms, creating a potentially large variety of VRAC channels with different properties. The variation of $I_{Cl(swell)}$ inactivation kinetics between different tissues and cells (*3*) can be ascribed to different expression ratios of LRRC8 isoforms. LRRC8-dependent Cl^- and taurine fluxes indicated that VRAC is identical to VSOAC (*6*) and fit to a pore formed by LRRC8 hexamers, because hexameric pannexin channels likewise display poor substrate specificity (*28*).

Our results provide the basis to explore the structure-function relationship of VRAC/VSOAC, to clarify the signaling pathway that couples cell volume increase to channel opening, and to investigate the role of the channel in basic cellular processes such as cell division, growth, and migration and in various pathological states. Interestingly, a truncating *LRRC8A* mutation has been described in a patient with agammaglobulinemia (*21*), and *LRRC8C* may have a role in fat metabolism (*31*).

References and Notes

1. E. K. Hoffmann, I. H. Lambert, S. F. Pedersen, *Physiol. Rev.* **89**, 193–277 (2009).
2. H. Pasantes-Morales, R. A. Lezama, G. Ramos-Mandujano, K. L. Tuz, *Am. J. Med.* **119** (suppl. 1), S4–S11 (2006).
3. B. Nilius *et al.*, *Prog. Biophys. Mol. Biol.* **68**, 69–119 (1997).
4. Y. Okada, K. Sato, T. Numata, *J. Physiol.* **587**, 2141–2149 (2009).
5. Y. Okada, *Am. J. Physiol.* **273**, C755–C789 (1997).
6. P. S. Jackson, K. Strange, *Am. J. Physiol.* **265**, C1489–C1500 (1993).
7. K. Strange, P. S. Jackson, *Kidney Int.* **48**, 994–1003 (1995).
8. I. H. Lambert, E. K. Hoffmann, *J. Membr. Biol.* **142**, 289–298 (1994).
9. D. B. Shennan, *Cell. Physiol. Biochem.* **21**, 15–28 (2008).
10. A. Stutzin *et al.*, *Am. J. Physiol.* **277**, C392–C402 (1999).
11. T. Moser, R. H. Chow, E. Neher, *Pflugers Arch.* **431**, 196–203 (1995).
12. Y. Okada *et al.*, *J. Membr. Biol.* **209**, 21–29 (2006).
13. S. Gründer, A. Thiemann, M. Pusch, T. J. Jentsch, *Nature* **360**, 759–762 (1992).
14. S. C. Stotz, D. E. Clapham, *PLOS ONE* **7**, e46865 (2012).
15. L. T. Chien, H. C. Hartzell, *J. Gen. Physiol.* **132**, 537–546 (2008).
16. R. Fischmeister, H. C. Hartzell, *J. Physiol.* **562**, 477–491 (2005).
17. L. J. Galietta, P. M. Haggie, A. S. Verkman, *FEBS Lett.* **499**, 220–224 (2001).
18. V. Benfenati *et al.*, *Channels* **3**, 323–336 (2009).
19. K. Kubota *et al.*, *FEBS Lett.* **564**, 147–152 (2004).
20. F. Abascal, R. Zardoya, *Bioessays* **34**, 551–560 (2012).
21. A. Sawada *et al.*, *J. Clin. Invest.* **112**, 1707–1713 (2003).
22. L. Cong *et al.*, *Science* **339**, 819–823 (2013).
23. B. Nilius, J. Prenen, U. Wissenbach, M. Bödding, G. Droogmans, *Pflugers Arch.* **443**, 227–233 (2001).
24. C. Y. Hernández-Carballo, J. A. De Santiago-Castillo, T. Rosales-Saavedra, P. Pérez-Cornejo, J. Arreola, *Pflugers Arch.* **460**, 633–644 (2010).
25. G. X. Wang *et al.*, *Am. J. Physiol. Heart Circ. Physiol.* **287**, H533–H544 (2004).
26. J. L. Leaney, S. J. Marsh, D. A. Brown, *J. Physiol.* **501**, 555–564 (1997).
27. G. Smits, A. V. Kajava, *Mol. Immunol.* **41**, 561–562 (2004).
28. S. Penuela, R. Gehi, D. W. Laird, *Biochim. Biophys. Acta* **1828**, 15–22 (2013).
29. S. Maeda *et al.*, *Nature* **458**, 597–602 (2009).
30. B. Nilius *et al.*, *Pflugers Arch.* **428**, 364–371 (1994).
31. T. Hayashi *et al.*, *Biol. Pharm. Bull.* **34**, 1257–1263 (2011).
32. M. Magrane, U. Consortium, *Database (Oxford)* **2011**, bar009 (2011).

Acknowledgments: We thank M. Neuenschwander for technical advice concerning the assay; H.-P. Rahn for help with fluorescence-activated cell sorting; A. Brockhoff and W. Meyerhof for use of their Fluorometric Image Plate Reader in a pilot experiment; and J. Liebold, N. Krönke, J. Jedamzick, and S. Kleissle for technical assistance. Supported by the European Research Council Advanced Grant (FP/2007-2013) 294435 "Cytovolion" and the Deutsche Forschungsgemeinschaft (Exc 257 "Neurocure") to T.J.J.

Supplementary Materials

www.sciencemag.org/content/344/6184/634/suppl/DC1
Materials and Methods
Author Contributions
Figs. S1 to S10
Tables S1 to S4
References (*33*–*38*)

3 March 2014; accepted 2 April 2014
Published online 10 April 2014;
10.1126/science.1252826

Gibberellin Acts Positively Then Negatively to Control Onset of Flower Formation in *Arabidopsis*

Nobutoshi Yamaguchi,[1] Cara M. Winter,[1]* Miin-Feng Wu,[1] Yuri Kanno,[2] Ayako Yamaguchi,[1] Mitsunori Seo,[2] Doris Wagner[1]†

The switch to reproductive development is biphasic in many plants, a feature important for optimal pollination and yield. We show that dual opposite roles of the phytohormone gibberellin underpin this phenomenon in *Arabidopsis*. Although gibberellin promotes termination of vegetative development, it inhibits flower formation. To overcome this effect, the transcription factor LEAFY induces expression of a gibberellin catabolism gene; consequently, increased LEAFY activity causes reduced gibberellin levels. This allows accumulation of gibberellin-sensitive DELLA proteins. The DELLA proteins are recruited by SQUAMOSA PROMOTER BINDING PROTEIN–LIKE transcription factors to regulatory regions of the floral commitment gene *APETALA1* and promote *APETALA1* up-regulation and floral fate synergistically with LEAFY. The two opposing functions of gibberellin may facilitate evolutionary and environmental modulation of plant inflorescence architecture.

Synchronization of the developmental transitions that lead to reproductive competence is important for species survival. Plants form new lateral organs iteratively throughout their life from the flanks of the shoot apical meristem (fig. S1) (*1*, *2*). The type of the lateral organ produced depends on the phase of the life cycle. In *Arabidopsis*, rosette leaves are produced during the vegetative phase. During the reproductive phase, an inflorescence forms. Not all lateral organ primordia of the inflorescence are competent to become flowers. Those that are not instead give rise to branches subtended by cauline leaves during the first inflorescence phase (*3*, *4*). The duration of the branch-producing first inflorescence phase determines inflorescence architecture and is critical for optimal seed set.

To gain insight into the regulation of the transition from branch to floral fate in the lateral primordia of the inflorescence, we analyzed public genome-wide binding and expression data and identified genes that are direct targets of the LEAFY (LFY) transcription factor (*5*–*7*) (table S1). LFY promotes flower formation (*8*, *9*). We identified for further study the *EUI-LIKE P450 A1* (*ELA1*) gene (fig. S2), which encodes a cytochrome P450 (*10*). *ELA1* expression was very low in vegetative tissues but increased when flowers formed (fig. S3). On the basis of in situ hybridization and reporter studies, *ELA1* was initially expressed on the abaxial side of incipient flower primordia and later along their entire circumference (Fig. 1A and fig. S3). *ELA1* expression was dependent on the

[1]Department of Biology, University of Pennsylvania, 415 South University Avenue, Philadelphia, PA 19104–6018, USA. [2]RIKEN Center for Sustainable Resource Science, Yokohama, Kanagawa, 230-0045, Japan.

*Present address: Department of Biology, Duke University, Box 90338, Durham, NC 27708, USA.
†Corresponding author. E-mail: wagnerdo@sas.upenn.edu